Spin-momentum locking in oxide interfaces and in Weyl semimetals

Bovenzi, N.

5 Phase shift of cyclotron orbits at type–I and type–II multi–Weyl nodes

5.1 Introduction

Electrons moving along cyclotron orbits in a homogeneous magnetic field are subject to the quantization condition [161]

$$l^2 S = 2\pi(m + \gamma), \quad m \in \mathbb{Z}, \tag{5.1}$$

where S is the zero-field area enclosed by the cyclotron orbit in momentum space, $l = \sqrt{\hbar/eB}$ is the magnetic length, and the offset γ includes quantum corrections, which can be expanded in powers of the magnetic field B [174]. In the semiclassical regime when the magnetic length is much larger than the Fermi wavelength, field-dependent corrections to γ are suppressed and the remaining number of zeroth order in B encodes valuable information about the electronic properties of the system. In particular, the offset includes contributions coming from topological features in the band structure [163–165], which makes it the subject of high current interest. Experimentally it can be deduced from quantum oscillations in the de Haas-van Alphen or the Shubnikov-de Haas effects, widely used nowadays to identify Weyl, Dirac, and nodal-line semimetals [175–179].

Interestingly, in some well-studied systems the offset measures the topological features independent of the specifics of the band structure. So, e.g., in graphene and graphene bilayer exposed to an out-of-plane magnetic field the offset turns out to be given by a winding number—the number of full turns made by the direction of the electron's pseudospin degree of freedom during a single turn around the cyclotron orbit [164]. This integer winding number is a robust feature, determined by the type of the band touching, and is sometimes called the topological charge of the Weyl or Dirac fermion [180]. In contrast to the common belief, however, the topological charge contributes to the offset in such a robust manner only in exceptional cases, namely when particular symmetry constraints are

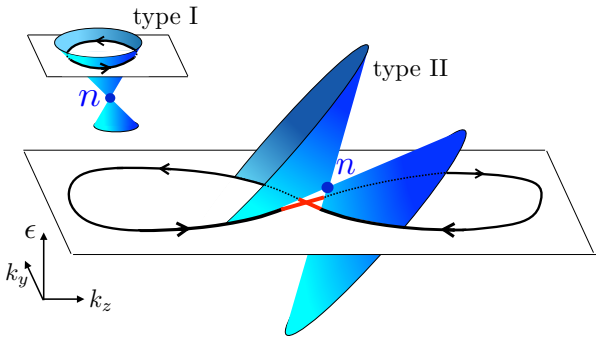

Figure 5.1: Schematic illustration of a breakthrough cyclotron orbit (figure-8 curve) at a type-II Weyl node with topological charge n. The red part indicates quantum tunneling in the magnetic-breakthrough region. The inset shows a cyclotron orbit at a type-I Weyl node.

satisfied [165]. In general, the offset is sensitive also to other parameters of the band touching and it is the aim of this work to characterize this sensitivity.

One important parameter is a linear tilt of the dispersion at the Weyl node, which is generically present in material realizations and, most importantly, leads to the occurrence of two types of Weyl nodes, as sketched in Fig. 5.1. Upon the type-I to type-II transition, the tilt exceeds a critical value, above which an equi-energy surface near the node cuts both bands [58]. The closed cyclotron orbit at a type-I Weyl node is thereby replaced by two open branches, which can be closed at large momenta by higher-order corrections to the Weyl Hamiltonian, resulting in two cyclotron orbits, one electron-like and one hole-like. Band details determine a critical magnetic field, above which the two separate cyclotron orbits effectively merge into a single orbit via magnetic breakthrough [181, 182]. This critical field is zero if the energy and the parallel momentum are exactly at the node where the two contours touch [81, 166], and is larger than zero if the gap between the contours is finite. The magnetic breakdown contributes an additional phase to the offset γ, so one would expect that the offset is even more sensitive to details of the orbit than in the case without magnetic breakdown.

In this work we analyze the offset for orbits at both types of Weyl nodes and find characteristic dependence of γ on the Weyl-node parameters. Most surprisingly, the offset of the breakthrough orbit at a type-II Weyl point turns out to depend only on the topological charge. This striking result is based on two facts, the universality of the phase jump of π acquired in

the magnetic-breakthrough region and a robust phase shift of $n\pi$ induced by the topological charge. The insensitivity of the latter on details of the orbit comes from a cancellation of a non-universal part of the phase in the two loops of the breakthrough orbit, which are traversed in opposite directions.

5.2 Model

We consider a set of Hamiltonians that govern the physics close to topologically distinct band touchings,

$$H_0 = k_-\sigma_+ + k_+\sigma_- + u\,k_z\sigma_0, \tag{5.2a}$$
$$H_n = k_-^n\sigma_+ + k_+^n\sigma_- + u\,k_z\sigma_0 + k_z\sigma_z,\ n \in \{1, 2, \dots\}, \tag{5.2b}$$

where $k_\pm = k_x \pm ik_y$, $(k_x, k_y, k_z) = \mathbf{k}$ are momenta (scaled by velocities), $\sigma_\pm = \sigma_x \pm i\sigma_y$, $\sigma_{x,y,z}$ are Pauli matrices, and σ_0 the identity matrix. The band touching at $\mathbf{k} = 0$ described by H_n corresponds to a topologically protected multi-Weyl node of order n [59], while H_0 describes a trivial, non-protected band touching (a gap is produced by a perturbation $\propto \sigma_z$). The parameter $u > 0$ controls the tilt of the Weyl cone; for $u < 1$ and $u > 1$ the Weyl cone is of type I and II, respectively.

The magnetic field pointing in x direction moves the particles along equi-energy contours $k_z(k_y)$ at fixed energy ϵ and parallel momentum component k_x. The contours are determined by the Schrödinger equation

$$H_n|u_{n\pm}\rangle = \epsilon|u_{n\pm}\rangle, \tag{5.3}$$

where $\pm$ denote the two bands.

In the quantization condition (5.1) one can distinguish three phase shifts that contribute to the offset

$$\gamma = \frac{1}{2\pi}(\phi_0 + \phi_\mathrm{b} + \phi_\mathrm{t}). \tag{5.4}$$

Here ϕ_0 and ϕ_b are phase shifts that occur at singular points on the orbit. Specifically, turning points give rise to the Maslov phase ϕ_0 [183], in which each turning point contributes a phase jump of $\pm\pi/2$, the sign determined by the sign of the curvature at the turning point. In particular one finds that $\phi_0 = \pi$ and $\phi_0 = 0$ for orbits that can be deformed into a circle and into an 8-shape, respectively. With ϕ_b we denote the phase shifts that occur due to magnetic breakdown. Finally, ϕ_t is the topological phase shift, which includes the Berry phase accumulated during a full turn around the

orbit and the effect of the orbital magnetic moment [163–165, 184]. The explicit calculation of ϕ_b and ϕ_t is the main result of this work, which will be presented in the following.

5.3 Topological phase shift

The topological phase shift of a closed contour at energy ϵ and the fixed momentum component k_x is given by [164, 185]

$$\phi_\mathrm{t} = \oint dk_y' \left[A - \frac{dk_z(k_y')}{d\epsilon} M \right]. \tag{5.5}$$

Here the first term is determined by the Berry connection projected onto the contour,

$$A = i\langle u|\nabla_\mathbf{k}|u\rangle \cdot \frac{d\mathbf{k}}{dk_y} = i\langle u|\frac{d}{dk_y}|u\rangle, \tag{5.6}$$

which contributes to ϕ_t the usual Berry phase of the closed orbit. The second term is the correction to the zero-field area S coming from the orbital magnetic moment projected onto the direction of the magnetic field [184],

$$\begin{aligned} M = \frac{i}{2}\Big[&\big(\partial_{k_y}\langle u|\big)\big(\epsilon - H\big)\big(\partial_{k_z}|u\rangle\big) \\ &- \big(\partial_{k_z}\langle u|\big)\big(\epsilon - H\big)\big(\partial_{k_y}|u\rangle\big)\Big]. \end{aligned} \tag{5.7}$$

The eigenfunctions of the Hamiltonian H_i can be written as

$$\begin{aligned} |u_{0\,\pm}\rangle &= \frac{1}{\sqrt{2}} \begin{pmatrix} \mp e^{-i\alpha} \\ 1 \end{pmatrix}, \\ |u_{n+}\rangle &= \begin{pmatrix} -\sin\frac{\beta}{2} e^{-in\alpha} \\ \cos\frac{\beta}{2} \end{pmatrix}, \quad |u_{n-}\rangle = \begin{pmatrix} \cos\frac{\beta}{2} e^{-in\alpha} \\ \sin\frac{\beta}{2} \end{pmatrix}, \end{aligned} \tag{5.8}$$

where the angles α and β are defined as

$$\begin{aligned} \cos\beta = \frac{k_z}{k}, \quad \sin\beta = \frac{\left(k_x^2 + k_y^2\right)^{\frac{n}{2}}}{k}, \\ \alpha = \mathrm{Arg}(k_x + ik_y), \quad k = \sqrt{\left(k_x^2 + k_y^2\right)^n + k_z^2}. \end{aligned} \tag{5.9}$$

For the topologically trivial case we obtain from (5.6)–(5.9)

$$A_{0\pm} = \frac{k_x}{2(k_x^2 + k_y^2)}, \quad M_{0\pm} = 0, \tag{5.10}$$

and the topological phase shift vanishes as it should,

$$\phi_{\rm t}^{\pm} = \oint dk'_y\, A_{0\pm} = \oint dk'_y \frac{k_x}{2[k_x^2 + (k'_y)^2]} = 0 \quad (n = 0), \tag{5.11}$$

independent of the integration contour. For the non-trivial case, we obtain

$$A_{n\pm} = \frac{nk_x\big(k_x^2 + k_y^2\big)^{n-1}}{2k(k \pm k_z)}, \;\; M_{n\pm} = -\frac{nk_x\big(k_x^2 + k_y^2\big)^{n-1}}{2k^2}. \tag{5.12}$$

To calculate the topological phase shift, we consider the explicit expression for the equi-energy contours, which is derived from (5.3) in the form

$$k_z^{\pm}(k_y) = \frac{\epsilon\, u \pm \sqrt{(u^2-1)\big(k_x^2 + k_y^2\big)^n + \epsilon^2}}{u^2 - 1}. \tag{5.13}$$

For $u > 1$, the contours given by $k_z^{\pm}(k_y)$ are disjoint and we need to introduce an additional orbit segment that connects the two open ends of $k_z^{\pm}(k_y)$ at $k_z \to \pm\infty$. These connecting segment can be realized by an additional mass term $\eta k_z^3 \sigma_z$ in the Hamiltonian, with an infinitesimal $\eta > 0$. The reconnection then occurs at large momenta k_z, with $|k_z| > (u-1)/\eta \to \infty$. In the expressions (5.12) for A and M the additional mass term replaces $k_z \to k_z + \eta k_z^3$. On the connecting segment, A and M go to zero like η^2, while the integration along the connecting segment gives a factor of order $1/\eta$. Hence the contribution of the connecting segment to $\phi_{\rm t}$ vanishes and the integration reduces to the integration along the main contour $k_z^{\pm}(k_y)$.

Inserting (5.12) and (5.13) into (5.5) we obtain

$$\phi_{\rm t}^{\pm} = \mp \int dk'_y \frac{(u+1)nk_x\big(k_x^2 + (k'_y)^2\big)^{n-1}}{2\big[k^{\pm} \pm k_z^{\pm}\big]\big[k_z^{\pm} \mp uk^{\pm}\big]}. \tag{5.14}$$

For a type-II cone ($u > 1$) we use the substitution $\kappa = k'_y/k_x$ and obtain

$$\begin{aligned}\phi_{\rm t}^{\pm} = & \int_{-\infty}^{\infty} d\kappa \frac{n(\kappa^2+1)^{n-1}}{2\sqrt{(\kappa^2+1)^n + \cot^2\theta}} \\ & \times \Big(\sqrt{(\kappa^2+1)^n + \cot^2\theta} \pm \cot\theta\Big)^{-1},\end{aligned} \tag{5.15}$$

where the parameter θ encoding contour details is defined as

$$\theta = \begin{cases} \operatorname{atan}\left(\frac{k_x^n\sqrt{u^2-1}}{\epsilon}\right) & u > 1 \\ \operatorname{atanh}\left(\frac{k_x^n\sqrt{1-u^2}}{\epsilon}\right) & u < 1. \end{cases} \tag{5.16}$$

The integral in (5.15) needs to be calculated numerically (see below); for the special case $n = 1$, we find the closed-form solution

$$\phi_{\mathrm{t}}^{\pm} = \frac{\pi}{2}(1 \mp \operatorname{sign}\theta) \pm \theta \qquad (n = 1). \tag{5.17}$$

While $\phi_{\mathrm{t}}^{\pm}$ are the topological phase shifts of the two (electron/hole) orbits $k_z^{\pm}(k_y)$, the sum $\phi_{\mathrm{t}}^{+} + \phi_{\mathrm{t}}^{-} \equiv \phi_{\mathrm{t}}^{\mathrm{br}}$ is the topological phase shift of the breakthrough orbit, i.e., the figure-of-8 orbit that encloses both the electron and the hole pocket. Using the substitution $z = (\kappa^2 + 1)^n$ the integral for $\phi_{\mathrm{t}}^{\mathrm{br}}$ simplifies to

$$\phi_{\mathrm{t}}^{\mathrm{br}} = \int_1^{\infty} dz \frac{1}{\sqrt{z^{\frac{2n+1}{n}} - z^2}} = n\pi, \tag{5.18}$$

where the θ dependent part cancels out. As a result the topological phase shift of the figure-of-8 orbit only depends on the quantized topological charge n, in contrast to the θ-dependent phase shifts of the separate orbits.

For type-I Weyl fermions ($u < 1$) $k_z^{\pm}$ are two parts of a single closed contour, which topological phase is denoted ϕ_{t}. A closed-form solution for the integral (5.14) is found for $n = 1$,

$$\phi_{\mathrm{t}} = \pi \operatorname{sign}\theta \qquad (n = 1), \tag{5.19}$$

in agreement with Refs. [164, 186–188]. For $n \geq 2$, we find in the limits $\theta \to 0^{\pm}$ and $\theta \to \pm\infty$,

$$\phi_{\mathrm{t}} \xrightarrow{=\theta\to 0^{\pm}} n\,\pi\,\operatorname{sign}\theta, \quad \phi_{\mathrm{t}} \xrightarrow{=\theta\to\pm\infty} \sqrt{n}\,\pi\,\operatorname{sign}\theta. \tag{5.20}$$

The full θ dependence will be discussed below.

5.4 Breakthrough phase shift

To calculate the additional phase shift of the figure-of-8 orbit due to magnetic breakdown, we follow a standard route [182] and calculate the

scattering matrix that relates the exact wavefunction of the magnetic-breakdown region with the in- and out-going semiclassical wavefunctions.

We start with the non-topological Hamiltonian H_0. Introducing the magnetic field via Peierls substitution $k_z \mapsto k_z + il^{-2}\partial_{k_y}$, followed by a unitary transformation,

$$\tilde{H}_0 = e^{-il^2(k_z-\epsilon/u)k_y} H_0 e^{il^2(k_z-\epsilon/u)k_y}, \tag{5.21}$$

we arrive at

$$\tilde{H}_0 = k_x\sigma_x + k_y\sigma_y + i\,u\,l^{-2}\partial_{k_y}\sigma_0 + \epsilon. \tag{5.22}$$

Rescaling the variables as $k = lk_y/\sqrt{u}$, $\delta_0 = lk_x/\sqrt{u}$, the Schrödinger equation $\tilde{H}_0\psi = \epsilon\psi$ reads

$$\big[\sigma_x\delta_0 + \sigma_y k + i\partial_k\big]\psi = 0. \tag{5.23}$$

The exact solution of (5.23) is known from the Landau-Zener problem [189]. To obtain the phase shift in comparison to the semiclassical solution of (5.23), the exact wavefunctions are matched with the incoming semiclassical wavefunctions at $k \ll -\delta_0$, denoted $\psi_i^{\pm}$, and outgoing $\psi_f^{\pm}$ at $k \gg \delta_0$. From this standard procedure (recapitulated in Sec. 5.7) we obtain the scattering matrix S that relates the final state in the basis (ψ_f^+, ψ_f^-) to the incoming state in the basis (ψ_i^+, ψ_i^-),

$$S = \begin{pmatrix} \sqrt{1-W}\,e^{i\alpha} & -i\sqrt{W} \\ -i\sqrt{W} & \sqrt{1-W}\,e^{-i\alpha} \end{pmatrix}, \tag{5.24}$$

where

$$W = e^{-\pi\delta_0^2}, \;\; \alpha = \tfrac{\pi}{4} + \tfrac{\delta_0^2}{2} - \tfrac{\delta_0^2}{2}\ln\tfrac{\delta_0^2}{2} + \arg\Gamma\Big(i\tfrac{\delta_0^2}{2}\Big). \tag{5.25}$$

The breakthrough orbit dominates if $\delta_0 \ll 1$, $W \approx 1$, in which case each band transition in the breakthrough region contributes a phase jump of $\pi/2$ giving in total the phase shift $\phi_{\rm b} = \pi$ for the breakthrough orbit.

For the topological case, we linearize the Hamiltonian H_n in k_y, leading to

$$H_n' = k_x^n\sigma_x + nk_x^{n-1}k_y\sigma_y + k_z\sigma_z + uk_z. \tag{5.26}$$

After Peierls substitution we apply the unitary transformation given by

$$\tilde{H}_n = e^{-il^2[k_z-\epsilon/(u^2-1)]k_y} H_n' e^{il^2[k_z-\epsilon/(u^2-1)]k_y}. \tag{5.27}$$

Rescaling and transforming the variables as

$$k = lk_y(u^2-1)^{-1/4}\sqrt{nk_x^{n-1}}, \tag{5.28a}$$

$$\delta_n = l\,\mathrm{sign}(\epsilon)\frac{\sqrt{\epsilon^2 + (u^2-1)k_x^{2n}}}{(u^2-1)^{3/4}k_x^{(n-1)/2}}, \tag{5.28b}$$

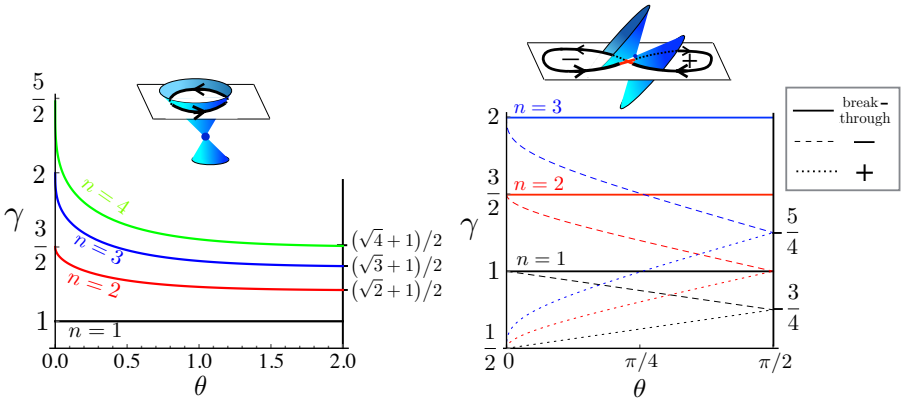

Figure 5.2: a) Parameter dependence of the offset γ of orbits at a type-I Weyl node. b) Parameter dependence of the offset γ of orbits at a type-II Weyl node. The offsets of separate orbits k_z^+ and k_z^- (without magnetic breakthrough) depend on the band parameter θ, while the offset of the figure-8 breakthrough orbit only depends on the topological charge n.

we obtain the Schrödinger equation

$$\Big[\delta_n\sqrt{u^2-1}\sin\theta\sigma_x + k\sqrt{u^2-1}\sigma_y + i\partial_k(u+\sigma_z) + \delta_n\cos\theta(1+u\sigma_z)\Big]\psi = 0. \tag{5.29}$$

Multiplying (5.29) from the left with $\mathcal{M} = \mathrm{diag}[(u+1)^{-1},(u-1)^{-1}]$ and applying a transformation given by

$$T = -i\begin{pmatrix} \frac{1-u}{\sqrt{u^2-1}} & \frac{u-1}{\sqrt{u^2-1}} \\ 1 & 1 \end{pmatrix}\sigma_z e^{-i\sigma_y\theta/2}, \tag{5.30}$$

we again arrive at the differential equation of the Landau-Zener form (5.23),

$$\hat{H}\hat{\psi}(k) = \big(\delta_n\,\sigma_x + k\,\sigma_y + i\partial_k\big)\hat{\psi}(k) = 0, \tag{5.31}$$

where $\hat{\psi}(k) = T^{-1}\psi(k)$ and $\hat{H} = T^{-1}\,\mathcal{M}\,\tilde{H}T$. The solution of (5.29) is thus given by the solution of the Landau-Zener problem multiplied from the left with the matrix T. Note that the θ phase brought into the full solution by the matrix T is the topological phase of the full solution induced by the non-trivial topology of the Hamiltonian.

The S matrix is obtained by matching $\psi(k)$ with the semiclassical solution of (5.29). Since H_n' is topologically equivalent to H_1 (note that the

dynamical variables are k_y and k_z, while k_x is fixed), the topological phase shift of the semiclassical solution is given by (5.17), which cancels the θ phase of the full solution and the result is the same θ-independent scattering matrix (5.24), with δ_0 replaced by δ_n. In particular, the breakthrough phase shift $\phi_\mathrm{b} = \pi$ also holds in the topological case.

5.5 Discussion

Having thus calculated the phase shifts, we now show the full θ-dependence of the offset γ, defined in Eq. (5.4), in Figs. 5.2a and 5.2b. In practice, the offset can only be measured modulo one, corresponding to one Landau-level spacing. Nevertheless in Figs. 5.2a and 5.2b we plot the full γ for clarity of the graphic. For the figure-of-8 orbit, the magnetic breakthrough contributes an offset $1/2$ and the topological charge adds an extra contribution $n/2$. The θ independence is based on the cancellation of the θ-dependent parts from the hole and the electron pockets. The universality of the breakthrough phase shift is, instead, less surprising, since the same universal value was found previously for non-topological band touchings [182]. In contrast, without breakthrough (dashed/dotted curves in Fig. 5.2b) or in case of a type-I Weyl node (Fig. 5.2a), the offset has a non-trivial dependence on the orbit details that are encoded in θ. The only exception is the case $n = 1$ of the type-I Weyl node, which shows no θ dependence owing to the higher symmetry of the dispersion [165]. This is also the only case with a known full quantum-mechanical solution [164, 186–188, 190, 191]; it agrees with our semiclassical result. In quantum oscillation experiments, the measured phase shift would likely be averaged over a range of values of the energy and of the parallel momentum k_x, corresponding to a weighted (depending on details of the experimental realization) average over the parameter θ. In general, this averaging does not destroy the θ dependence, still allowing to discriminate the two cases of quantized and continuously varying γ.

With regard to the figure-8 breakthrough orbits, our calculations explain recent numerical findings for the offset of a thin-film Weyl semimetal [192] and a type-II Weyl semimetal [81], showing, respectively, $\gamma = 1/2$ and $\gamma = 0$. In the case of the thin film, the Hamiltonian at the figure-8 crossing, given in the appendix of Ref. [192], is equivalent to the non-topological Hamiltonian H_0, thus the only phase contributing is the breakthrough phase $\phi_\mathrm{b} = \pi$, which explains the offset $\gamma = \phi_\mathrm{b}/2\pi = 1/2$. In case of the type-II Weyl semimetal, the Hamiltonian is equivalent to H_1, where the additional topological phase $\phi_\mathrm{t} = \pi$ cancels the breakthrough phase, which

explains the vanishing offset. This contradicts a previous interpretation that relates the vanishing offset of the latter to a vanishing Berry phase and neglects the contribution of the breakthrough phase [166]. In Appendix 5.8 we present extensions of the numerical calculations to the cases $n = 2$ and $n = 3$, tilted type-I Weyl cones, and several values of θ. Also these calculations are in agreement with the analytical results of this work.

5.6 Appendix A. Topological phases

Type-II ($u > 1$)

While the sum of the phases $\phi_{\mathrm{t}}^{\pm}$ has been calculated in the main text, to obtain each of the phases separately we now focus on the difference. From (5.15) we find

$$\phi_{\mathrm{t}}^{-} - \phi_{\mathrm{t}}^{+} = \int_{-\infty}^{\infty} d\kappa \frac{n \cot\theta}{(\kappa^2+1)\sqrt{(\kappa^2+1)^n + \cot^2\theta}}. \tag{5.32}$$

Using the series expansion

$$\frac{1}{\sqrt{1+q}} = \sum_{m=0}^{\infty} \binom{m-\frac{1}{2}}{m} (-q)^m \tag{5.33}$$

and the integral

$$\int_{-\infty}^{\infty} d\kappa \frac{1}{(\kappa^2+1)^{\alpha}} = \frac{\sqrt{\pi}\,\Gamma\left(\alpha-\frac{1}{2}\right)}{\Gamma(\alpha)}, \tag{5.34}$$

Eq. (5.32) can be written as

$$\begin{aligned}\phi_{\mathrm{t}}^{-} - \phi_{\mathrm{t}}^{+} = n\cot\theta \sum_{m=0}^{\infty} (-1)^m \binom{m-\frac{1}{2}}{m} \\ \times \frac{\sqrt{\pi}\,\Gamma\left(nm+\frac{n+1}{2}\right)}{\Gamma\left(nm+\frac{n+2}{2}\right)} (\cot\theta)^{2m}.\end{aligned} \tag{5.35}$$

For $n = 1$ the series is the expansion of $2\arctan(\cot\theta)/\cot\theta$, which gives

$$\phi_{\mathrm{t}}^{-} - \phi_{\mathrm{t}}^{+} = \mathrm{sign}(\theta)\pi - 2\theta. \tag{5.36}$$

Together with (5.18), $\phi_{\mathrm{t}}^{-} + \phi_{\mathrm{t}}^{+} = n\pi$, this leads to

$$\phi_{\mathrm{t}}^{\pm} = \frac{\pi}{2}(1 \mp \mathrm{sign}\theta) \pm \theta. \tag{5.37}$$

Type-I ($u < 1$)

For $u < 1$, $k_z^{\pm}$ are two parts of a single closed contour. The phase $\phi_{\rm t}$ of the contour is thus given by the difference $\phi_{\rm t} = \phi_{\rm t}^{+} - \phi_{\rm t}^{-}$, where, using (5.14), (5.16), and the substitution $\kappa = k_y'/k_x$, $\phi_{\rm t}^{\pm}$ are given by

$$\phi_{\rm t}^{\pm} = -\int_{-\kappa_0}^{\kappa_0} d\kappa \frac{n(\kappa^2+1)^{n-1}}{2\sqrt{\coth^2\theta - (\kappa^2+1)^n}} \Big(\sqrt{\coth^2\theta - (\kappa^2+1)^n} \pm \coth\theta\Big)^{-1}, \tag{5.38}$$

where $\kappa_0 = \sqrt{(\coth\theta)^{2/n} - 1}$. The difference reduces to

$$\phi_{\rm t} = \int_{-\kappa_0}^{\kappa_0} d\kappa \frac{n \coth\theta}{(\kappa^2+1)\sqrt{\coth^2\theta - (\kappa^2+1)^n}} \tag{5.39}$$

and, after the substitution $z = (\kappa^2+1)^n$, can be rewritten as

$$\phi_{\rm t} = \int_{1}^{\coth^2\theta} dz \frac{\coth\theta}{z\sqrt{\coth^2\theta - z}\sqrt{z^{1/n}-1}}. \tag{5.40}$$

A closed-form solution is found for $n = 1$,

$$\phi_{\rm t} = \pi\, \mathrm{sign}\theta. \tag{5.41}$$

For a general n we find in the limits $\theta \to 0^{\pm}$

$$\phi_{\rm t} \xrightarrow{\theta\to 0^{\pm}} n\,\pi\,\mathrm{sign}\theta \tag{5.42}$$

and $\theta \to \pm\infty$

$$\phi_{\rm t} \xrightarrow{\theta\to \pm\infty} \sqrt{n}\,\pi\,\mathrm{sign}\theta. \tag{5.43}$$

5.7 Appendix B. Scattering matrix for magnetic breakdown

Non-topological Hamiltonian

To obtain the full solution in the magnetic-breakthrough region, we solve the differential equation

$$\big[\sigma_x \delta + \sigma_y k + i\partial_k\big]\psi = 0. \tag{5.44}$$

Multiplying from the left with $U = \exp(-i\sigma_x\pi/4)$ and inserting the ansatz $\psi = U^\dagger(\eta, \xi)^T$ we obtain

$$\big(k^2 + \partial_k^2 - i + \delta^2\big)\eta = 0, \tag{5.45}$$

$$\xi = -\delta^{-1}\big(k + i\partial_k\big)\eta. \tag{5.46}$$

Equation (5.45) can be transformed to Weber's equation for the parabolic cylinder function,

$$\eta'' - \big(\tfrac{1}{4}z^2 + a\big)\eta = 0, \tag{5.47}$$

where

$$z = \sqrt{2}e^{i\pi/4}\,k, \quad a = \tfrac{1}{2} + i\gamma, \quad \gamma = \tfrac{1}{2}\delta^2. \tag{5.48}$$

The two solutions read

$$\eta_a = e^{-z^2/4}\ {}_1F_1\big(\tfrac{1}{2}a + \tfrac{1}{4}; \tfrac{1}{2}; \tfrac{1}{2}z^2\big), \tag{5.49a}$$

$$\eta_b = z\,e^{-z^2/4}\ {}_1F_1\big(\tfrac{1}{2}a + \tfrac{3}{4}; \tfrac{3}{2}; \tfrac{1}{2}z^2\big), \tag{5.49b}$$

where ${}_1F_1()$ is the confluent hypergeometric function. Its general asymptotic form for a large last argument reads

$${}_1F_1(\alpha, \beta, ik^2) \xrightarrow{k\to\infty} \Gamma(\beta)\Big(\tfrac{1}{\Gamma(\alpha)}e^{ik^2}(ik^2)^{\alpha-\beta} + \tfrac{1}{\Gamma(\beta-\alpha)}(-ik^2)^{-\alpha}\Big). \tag{5.50}$$

From this we obtain the asymptotic form of the two solutions (5.49),

$$\eta_a = \frac{\Gamma\big(\frac{1}{2}\big)}{\Gamma\big(\gamma\frac{i}{2} + \frac{1}{2}\big)}e^{ik^2/2 + i\gamma\ln|k| - \pi\gamma/4}, \tag{5.51a}$$

$$\eta_b = \mathrm{sign}(k)\,\frac{\sqrt{2}\Gamma\big(\frac{3}{2}\big)}{\Gamma\big(\gamma\frac{i}{2} + 1\big)}e^{ik^2/2 + i\gamma\ln|k| - \pi\gamma/4}. \tag{5.51b}$$

Inserting into (5.46), we obtain the two corresponding expressions for ξ,

$$\xi_a = -\,\mathrm{sign}(k)\,\frac{\sqrt{2\pi/\gamma}}{\Gamma\big(-\gamma\frac{i}{2}\big)}e^{-ik^2/2 - i\gamma\ln|k| + i\,\pi/4 - \pi\gamma/4}, \tag{5.52a}$$

$$\xi_b = -\,\frac{\sqrt{\pi/\gamma}}{\Gamma\big(\frac{1}{2} - \gamma\frac{i}{2}\big)}e^{-ik^2/2 - i\gamma\ln|k| + i\,3\pi/4 - \pi\gamma/4}. \tag{5.52b}$$

Altogether, an arbitrary solution of (5.44) at $|k| \gg \delta$ is thus the linear combination

$$\psi(k) = e^{i\sigma_x\pi/4}\Psi(k)\boldsymbol{a}, \quad \Psi(k) = \begin{pmatrix}\eta_a & \eta_b\\ \xi_a & \xi_b\end{pmatrix}, \quad \boldsymbol{a} = \begin{pmatrix}a_1\\ a_2\end{pmatrix}, \tag{5.53}$$

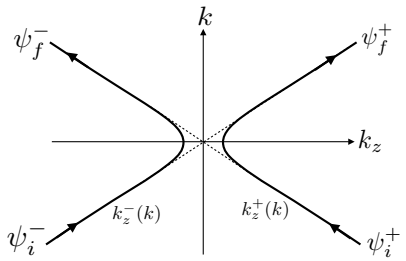

Figure 5.3: Classical trajectories along the equi-energy contours $k_z^{\pm}(k)$ approaching and leaving the magnetic-breakdown region. The in- and outgoing scattering states, $\psi_i^{\pm}$ and $\psi_f^{\pm}$, respectively, are also indicated.

where a_1, a_2 are arbitrary coefficients.

The approximate semiclassical solution of (5.44) reads [182, 193]

$$\psi_s(k) = \chi(k)\, e^{-i\int_0^k dk' k_z(k') + \phi_{\rm t}(k)}, \tag{5.54}$$

where $\chi(k)$ and $k_z(k)$ are determined by

$$\big[\sigma_x\delta + \sigma_y k + k_z^{\pm}(k)\big]\chi_{\pm}(k) = 0, \tag{5.55}$$

$$k_z^{\pm}(k) = \pm\sqrt{k^2+\delta^2} \tag{5.56}$$

and $\phi_{\rm t}(k)$ is the topological phase shift accumulated on the orbit section between $k_y = 0$ and $k_y = k$,

$$\begin{aligned}\phi_{\rm t}(k) &= i\int_0^k dk'_y\, \chi_{\pm}^{\dagger}(k)\partial_k\chi_{\pm}(k) = \int_0^k dk' \frac{\delta}{2(\delta^2+(k')^2)} \\ &= \arctan(k/\delta)/2.\end{aligned} \tag{5.57}$$

The first term in the exponent of the semiclassical wavefunction can be written as

$$\int_0^k dk' k_z^{\pm}(k') = \pm\,\mathrm{sign}(k) f(k) + \mathcal{O}\big(\delta_0^2/k^2\big), \tag{5.58a}$$

$$f(k) = \tfrac{1}{2}\big[k^2 + \delta_0^2\big(\ln|2k/\delta_0| + 1/2\big)\big]. \tag{5.58b}$$

The basis for the scattering matrix is formed by the semiclassical wavefunctions at $k \ll -\delta$ as incoming states ψ_i and at $k \gg \delta$ as outgoing states

ψ_f, as indicated in Fig. 5.3. To leading order in δ/k we obtain

$$\psi_i^{\pm} = e^{\pm i f(k)} \frac{1}{\sqrt{2}} \begin{pmatrix} \mp e^{i\pi/4} \\ e^{-i\pi/4} \end{pmatrix}, \tag{5.59}$$

$$\psi_f^{\pm} = e^{\mp i f(k)} \frac{1}{\sqrt{2}} \begin{pmatrix} \mp e^{-i\pi/4} \\ e^{i\pi/4} \end{pmatrix} \tag{5.60}$$

and combine the scattering states into matrices,

$$\Psi_i(k) = (\psi_i^+, \psi_i^-), \qquad \Psi_f(k) = (\psi_f^+, \psi_f^-). \tag{5.61}$$

We choose the coefficients of the full solution, $\boldsymbol{a}$, such that at $k_y \ll -\delta$ the full solution coincides with the incoming state, $\Psi_i \boldsymbol{c}_i$, where according to (5.61), $\boldsymbol{c}_i = (1,0)$ corresponds to incoming state ψ_i^+ and $\boldsymbol{c}_i = (0,1)$ corresponds to incoming state ψ_i^-. At $k \gg \delta$ the phase and amplitude of the final states, combined in $\boldsymbol{c}_f$, is then determined by matching $\psi(k)$ with $\Psi_f \boldsymbol{c}_f$. Altogether, the matching conditions read

$$\Psi_i(k \ll -\delta)\boldsymbol{c}_i = \Psi(k \ll -\delta)\boldsymbol{a}, \tag{5.62}$$

$$\Psi(k \gg \delta)\boldsymbol{a} = \Psi_f(k \gg \delta)\boldsymbol{c}_f. \tag{5.63}$$

Eliminating $\boldsymbol{a}$ we obtain the expression for the scattering matrix S

$$\boldsymbol{c}_f = \underbrace{\Psi_f(k)^{-1}\Psi(k)\Psi^{-1}(-k)\Psi_i(-k)}_{\equiv S}\boldsymbol{c}_i, \quad k/\delta \to +\infty. \tag{5.64}$$

Inserting the expressions $\Psi_f(k)$, $\Psi_i(k)$, and $\Psi(k)$ given above, we obtain the scattering matrix (5.24) given in the main text.

Topological Hamiltonian

We consider the Schrödinger equation

$$\Big[\delta_n \sqrt{u^2-1}\sin\theta\sigma_x + k\sqrt{u^2-1}\sigma_y + i\partial_k(u+\sigma_z) + \delta_n\cos\theta(1+u\sigma_z)\Big]\psi = 0. \tag{5.65}$$

The semiclassical solution reads

$$\psi_s(k) = \chi(k)\, e^{-i\int_0^k dk' k_z(k') + \phi_{\mathrm{t}}(k)}, \tag{5.66}$$

where $\chi(k)$ and $k_z(k)$ are given by

$$\Big[\delta_n\sqrt{u^2-1}\sin\theta\sigma_x + k\sqrt{u^2-1}\sigma_y + k_z^{\pm}(k)(u+\sigma_z) + \delta_n\cos\theta(1+u\sigma_z)\Big]\chi_{\pm}(k) = 0, \tag{5.67}$$

$$k_z^{\pm}(k) = \pm\sqrt{k^2+\delta_n^2}. \tag{5.68}$$

The phase $\int_0^k dk' k_z^{\pm}(k')$ is in analogy to the non-topological case given by (5.58) (with δ_0 replaced by δ_n). The topological phase shift is most easily obtained by considering the original Schrödinger equation

$$H_n'\psi = \epsilon\psi, \tag{5.69}$$

$$H_n' = k_x^n\sigma_x + nk_x^{n-1}k_y\sigma_y + k_z\sigma_z + uk_z, \tag{5.70}$$

which is related to (5.65) by a k_z shift introduced in (5.27) in the main text, which leaves the phase shift accumulated between $k=0$ and $k=\pm\infty$ invariant. The Hamiltonian is of the form of H_1. The topological phase shift thus calculates in analogy to the phase $\phi_{\mathrm{t}}^{1\pm}$ of the main text. Since by symmetry the phase shift from $k=0$ to $k=\pm\infty$ is half the phase shift from $k=-\infty$ to $k=\infty$, we can use Eq. (5.17) to obtain

$$\phi_{\mathrm{t}}^{n\pm}(k=\infty) = \frac{\pi}{4}(1\mp\mathrm{sign}\theta) \pm \frac{\theta}{2}, \tag{5.71}$$

which is sufficient for the in- and outgoing states at $k=\pm\infty$. Together with the spinors from (5.67) the scattering states read

$$\psi_i^{\pm} = e^{\pm if(k) - i\frac{\pi}{4}(1\mp\mathrm{sign}\theta)\mp i\theta/2}\begin{pmatrix}\mp i\sqrt{\frac{u-1}{2u}}\\ \sqrt{\frac{u+1}{2u}}\end{pmatrix}, \tag{5.72a}$$

$$\psi_f^{\pm} = e^{\mp if(k) + i\frac{\pi}{4}(1\mp\mathrm{sign}\theta)\pm i\theta/2}\begin{pmatrix}\pm i\sqrt{\frac{u-1}{2u}}\\ \sqrt{\frac{u+1}{2u}}\end{pmatrix}. \tag{5.72b}$$

To find the full solution $\psi(k)$ we multiply (5.65) from the left with $\mathcal{M} = \mathrm{diag}[(u+1)^{-1},(u-1)^{-1}]$ and apply a transformation given by

$$T = -i\begin{pmatrix}\frac{1-u}{\sqrt{u^2-1}} & \frac{u-1}{\sqrt{u^2-1}}\\ 1 & 1\end{pmatrix}\sigma_z e^{-i\sigma_y\theta/2}, \tag{5.73}$$

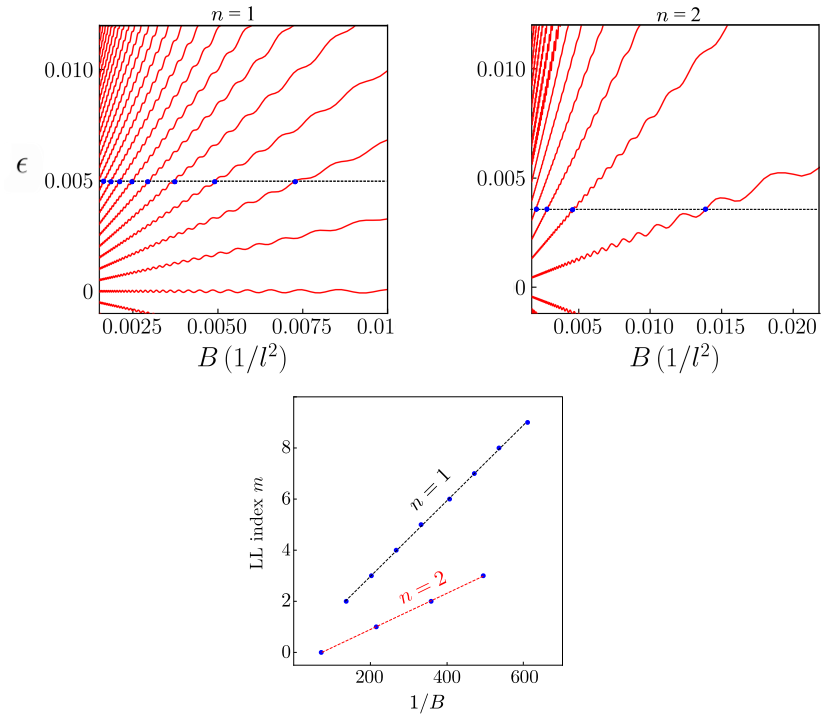

Figure 5.4: (a) Landau fan diagrams for type II Weyl nodes with topological charge $n = 1$ (left) and $n = 2$ (rigth) at $k_x = 0.005$ and $k_x = 0.03$, respectively. Other parameters are $u = 1.6$, $\eta = 0.1$, and $N_{cut} = 2400$. (b) Landau-level (LL) index m as a function of the inverse field for $n = 1, 2$ at fixed energies indicated by the black dashed lines in (a). The dots correspond to the numerical data, the dashed lines to the linear fits according to Eq. (5.77).

which leads to the differential equation of the Landau-Zener form (5.44),

$$\hat{H}\hat{\psi}(k) = \big(i\partial_k\sigma_0 + \delta_n\,\sigma_x + k\,\sigma_y\big)\hat{\psi}(k) = 0, \tag{5.74}$$

where $\hat{\psi}(k) = T^{-1}\psi(k)$ and $\hat{H} = T^{-1}\,\mathcal{M}\,\tilde{H}T$. As in the non-topological case, we obtain the S matrix by matching the full solution with the scattering states, $T^{-1}\psi^{\pm}_{i/f}$, which leads to the scattering matrix (5.24) with δ_0 replaced by δ_n.

5.8 Appendix C. Numerical results

To give support to the analytical calculations, we numerically compute the offset γ for type I and type II single, double, and triple Weyl nodes via numerical diagonalization of the Hamiltonian $H'_n = H_n(\boldsymbol{k'}) + \eta {k'_z}^3 \sigma_z$, with H_n given by Eq. (5.2b) of the main text, and the regularizing term $\eta {k'_z}^3 \sigma_z$ to ensure closed Fermi pockets in the case $u > 1$, as discussed in the main text. The magnetic field in the x direction enters according to the Peierls substitution $\boldsymbol{k'} = \boldsymbol{k} + \boldsymbol{A}$, with

$$k'_x = k_x, \;\; [k'_y, k'_z] = -iB\,. \tag{5.75}$$

We make use of the ladder operators a and $a^\dagger$ of the quantum oscillator to construct momentum operators with the required properties. Straightforwardly,

$$k'_y = (a + a^\dagger)\sqrt{\frac{B}{2}}, \;\; k'_z = i(a - a^\dagger)\sqrt{\frac{B}{2}} \tag{5.76}$$

with $[a, a^\dagger] = 1$, fulfil the commutator in Eq. (5.75).

The ladder operators are calculated in the basis of the Landau-level eigenstates (eigenstates of $a^\dagger a$), yielding the matrix elements $(a)_{ij} = \delta_{i,j+1}\sqrt{j}$ and $(a^\dagger)_{ij} = \delta_{i,j-1}\sqrt{i}$, respectively. The lowest l Landau levels are obtained by sparse diagonalization of the Hamiltonian constructed from ladder operators truncated to $i, j \in [1, N_{cut}]$ with $N_{cut} \gg l$, ensuring convergence of the eigenvalues with the value of N_{cut}.

The fan diagrams, shown in Fig. 5.4, are obtained by repeating this procedure at different values of the magnetic-field strength. For type-II Weyl orbits the limit of unit breakthrough probability is never achieved in practice, resulting in non-monotonic contribution to Landau-level energies [182, 193], producing oscillations on top of the fans in Fig. 5.4. These, however, are not the subject of our present analytical study. Therefore, in order to better extract the phase shift, we suppress these oscillations for $n = 2$ and $n = 3$ by averaging the energies over a range of magnetic fields containing several oscillation peaks (dips).

At a fixed energy ϵ, we extract the intercept fields $\{B_m\}$, where B_m is the value of the field at which the energy of the mth Landau level equals ϵ. The inverse of the intercept fields are then fitted to the quantization condition, Eq. (5.1) of the main text,

$$\frac{1}{B_m} = \frac{2\pi}{S(\epsilon)}(m + \gamma)\,, \tag{5.77}$$

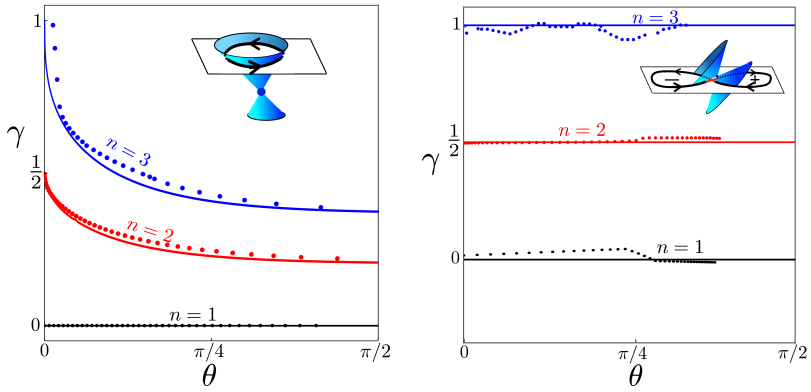

Figure 5.5: Parameter dependence of the offset γ (modulo one) for cyclotron orbits at type-I (left) and type-II (right) Weyl nodes obtained numerically (dots), compared to the analytical results (solid lines) of the main text [cf. Figs. 5.2a and 5.2b]. Parameters for numerical results are $u = 1.6$ ($u = 7$), $\eta = 0.1$ ($\eta = 1$), and $N_{cut} = 2400$ ($N_{cut} = 800$) for $n = 1, 2$ ($n = 3$). The relatively large value of u and η for $n = 3$ were necessary to access large values of θ [cf. Eq. (5.16)], at the same time closing the contour at not too large momenta.

where the zero-field area $S(\epsilon)$ enclosed by the equi-energy contour is calculated numerically from the dispersion at $B = 0$. The offset γ modulo one is thus obtained as the only fitting parameter.

The results, shown in Fig. 5.5, are in good agreement with the analytical results presented in the previous sections, for all the cases that we were able to address numerically. The phase offset $\gamma = 1/2$ corresponding to the non-protected band-touching Hamiltonian (5.2a) was obtained numerically in the context of figure-8 cyclotron orbits in a thin-film Weyl semimetal [192], also in agreement with the analytical results of this chapter.